Shift and torsion contact problems for arbitrary axisymmetric normal stress distributions

CrossMark

G.Sh. Boltachev [a], V. Aleshin [b],*

[a] Institute of Electrophysics, Ural Division, Russian Academy of Sciences, 106 Amundsen St., 620016 Ekaterinburg, Russia
[b] Joint European Laboratory LEMAC, Institut d'Electronique, de Microélectronique et de Nanotechnologie (IEMN-DOAE UMR CNRS 8520), Avenue Poincaré-BP 60069, 59652 Villeneuve d'Ascq Cedex, France

ABSTRACT

In this paper, we analyze the contact interaction of axisymmetric particles subject to a subsequent application of a constant normal load and a tangential or rotational force. A rigorous solution to the frictional contact problem is given by the known Jäger theorem that presents a relationship between shear and normal stress distributions provided the latter is an exact solution to a normal contact problem. However, in the case of strong loading, when the normal displacement reaches a value of 5–10% of the spheres' diameter, exact solutions for the normal problem are absent; some model concepts exist instead. For instance, the rod model describes strong normal loading of spheres as a sort of combination of the Hertz problem (weak loading of spheres) with a compression of a pair of confined cylinder of the same radius as the Hertz contact spot. Here we propose a method that is based on considerations similar to the Jäger theorem but is appropriate for any model (or empirical) normal stress distribution. The resulting integral representations describe both shearing and torsion of prestressed particles with axisymmetric profiles. Rolling of particles, as well as plasticity and adhesion of the particles' material, are not considered. We also analyze the asymptotic behavior of the integral representations for weak and strong strains. The obtained general solutions allow us to use the method of memory diagrams in order to calculate the reaction of the system on arbitrarily varying tangential or rotational actions.

1. Introduction

The contact interaction problem for elastic solids is of interest from the point of various applications and related theories, such as collision of bodies, soil and rock mechanics, dynamics of powders and granular materials, etc. (see, for instance books by Mavko et al. (1998), Duran (1999), Capriz et al. (2008)). When two spheres are compressed together a round contact spot appears and a repulsive force N arises. For a weak compression, when the contact radius a is much less than the spheres diameter d, the solution to the normal contact problem was published by Hertz (1881):

$$N = \frac{1}{3} \frac{Ed^2}{1-v^2} \left(\frac{h}{d}\right)^{3/2} \tag{1a}$$

$$a = \frac{1}{2}(hd)^{1/2} \tag{1b}$$

$$\sigma(a,\rho) = \begin{cases} -\frac{4E}{\pi d(1-v^2)}(a^2 - \rho^2)^{1/2}, & \rho < a \\ 0, & \rho \geqslant a \end{cases} \tag{1c}$$

where h is the total normal displacement of the spheres' centers (the centers are defined in the unstrained state and are supposed not to shift during straining), E is the Young modulus, v is the Poisson coefficient, $\sigma(a,\rho)$ is the radial distribution of the normal stress on the contact spot.

Application of a tangential force T in a system with friction results in the appearance of the shear stress τ defined on the same contact spot, in which two zones has to be distinguished: the zone of stick ($\rho \leqslant b$) where no relative shift between the interfaces is created, and the zone of slip ($b < \rho \leqslant a$) where the Coulomb friction law with the friction coefficient μ is postulated, $\tau = \mu\sigma$. The shear stress (traction) distribution was calculated by Cattaneo (1938) and Mindlin (1949) by using the known *Boussinesq* and Cerruti solutions for an elastic half-space deformed by a point force. Jäger (1995) proposed a different, more compact method based on rigid punch solutions i.e. on the approximation of a deformed profile by a series of infinitesimal flat circular punch-like displacements with a known solution for each of them. The technique allows one to avoid singular integrals (Jäger, 2002) typical for methods that use

* Corresponding author. Tel.: +33 320 19 79 49; fax: +33 320 34 87 50.
  E-mail address: vladislav.aleshin@iemn.univ-lille1.fr (V. Aleshin).

concentrated forces, and, finally, to reduce the tangential problem to the normal one. Indeed, the resulting traction distribution

$$\tau(\rho) = \mu[\sigma(a,\rho) - \sigma(b,\rho)] \tag{2}$$

is expressed through the normal stress. Eq. (2) can be supplemented by an analogous expression for the tangential displacements, both local (ρ-dependent) and global ones (maximum local). This result is known as the Jäger theorem or the Jäger elastic principle. In the derivation, the particular form of the dependency $\sigma(a,\rho)$, such as the Hertz solution Eq. (1c), is not used. The general form Eq. (2) follows from the identical representation of Green's functions for normal and tangential loading of an elastic half-space (see, for instance, Barber et al., 2011). Therefore, the result Eq. (2) is valid for any normal stress distribution on condition that the latter presents a solution for some elastic loading problem in which the loaded body can be locally approximated by a half-space.

2. High contact stresses and rod model

In that way, the Jäger theorem allows one to obtain solutions to the friction problem for various contact geometries. However, the method required the knowledge of the exact normal stress distribution that, in practice, leads to a restriction on weakness of deformation. At the same time, it has been confirmed (Jefferson et al., 2002; Dintwa et al., 2008)[1] that the Hertz solution considerably underestimates the elastic repulsion force in the case of finite strains $h/d > 0.01$. The limited applicability of the Hertz solution becomes a serious problem in granular dynamics simulations for compaction of nano-powders with typical deformations h/d of about 5–10% (see Boltachev et al., 2011; Boltachev and Volkov, 2012). At such high strains, deformation of a particle due to its contact with one selected neighbor affect considerably its global shape and thus influences contacts with all remaining neighbors (Jefferson et al., 2002). An analytical solution to that problem is hardly possible. Even the normal problem of two diametrically opposite contacts has not been rigorously solved yet. In this situation, approximate but physically correct models extrapolating the Hertz solution are particularly important. A possible extrapolation is presented by the rod model (Boltachev and Volkov, 2012; Boltachev et al., 2012) that results in

$$N = \frac{1}{3}\frac{Ed^2}{1-v^2}\left(\frac{h}{d}\right)^{3/2} - \frac{\pi}{4}\frac{Ed^2(1-v)}{(1-2v)(1+v)}\left[\frac{h}{d} + ln\left(1 - \frac{h}{d}\right)\right] \tag{3a}$$

$$a = \frac{1}{2}(hd)^{1/2} \tag{3b}$$

$$\sigma(a,\rho) = -\frac{4E}{\pi d(1-v^2)}(a^2 - \rho^2)^{1/2}$$
$$-\frac{E(1-v)}{(1-2v)(1+v)}ln\left(\frac{d^2 - 4\rho^2}{d^2 - 4a^2}\right) \tag{3c}$$

The rod model is based on the idea that, for high strains, the deformation of spheres occurs not only in vicinity of contact, as in the Hertz mechanics, but involves deeper layers of the material.

Fig. 1. In the rod model, high deformation of spheres is presented as the sum of the Hertz solution and the uniaxial confined compression of two cylinders.

The simplest representation of these deeper layers can be obtained by replacing them by the uniaxial deformation of cylinders with the same radius as the radius of contact (see Fig. 1). The cylinders are supposed to be confined so that they cannot expand in the lateral direction. The latter agrees to the fact that the virtually cut cylinders with the axis connecting the spheres' centers are surrounded by the bulk material of spheres. It is supposed that the relation Eq. (3b) between the contact radius and normal displacement is the same as Eq. (1b) for Herzian spheres. The rod model has two major advantages: the model dependency $N(h)$ agrees well with the FEM simulations by Dintwa et al. (2008) and behaves correctly for both small and high strains. Indeed, $h/d \ll 1$ the solution (3a), (3b), (3c) tends to the Hertz solution (1a), (1b), (1c), while for $h/d \to 1$ the loading-displacement curve $N(h)$ has a singularity that guarantees, in contrast to the Hertz law, the impossibility of overlapping particles centers.

An important limitation of the rod model is related to the Poisson coefficient that should not be too close to 0.5. Indeed, a virtual addition of confined cylinders mean that their lateral deformation is prohibited or at least hampered by the remaining ring-like parts of the spheres. This is not the case when $v = 0.5$ and the lateral expansion of the cylinders is essential; moreover, assuming $v = 0.5$ results in singularities in Eqs. (3a) and (3c). A more precise analysis would require a more sophisticated dependence between the contact radius and cylinders' radius than a simple equality and, finally, the account for deformation of the remaining ring-like parts. Without pretending to provide a strict description, we just stress that the rod model provides a better approximation than the Hertz solution for finite values of h/d and for materials having behavior different from the "incompressible" limit $v = 0.5$.

Since the resulting expressions of the rod model do not correspond exactly to any rigorous solution for a contact problem, the Jäger theorem does not apply in that case. The problem of the tangential shift for particles that support the stress distribution (3c) in the contact zone is solved by Boltachev et al. (2012) by means of Mindlin's methodology, i.e. by using known solutions for a point force applied to an elastic half-space. The final expression for traction τ is quite cumbersome; the tangential load–displacement relation $T(\delta)$ i.e. the dependency of the total tangential force T on the tangential shift δ of each particle relative to their contact spot is given by

$$\frac{\delta}{\mu d} = \frac{2-v}{1-v}\frac{a^2-b^2}{d^2} + \frac{(2-v)(1-v)}{1-2v}\psi(a,b), \tag{4a}$$

$$\frac{T}{\mu Ed^2} = \frac{8}{3d^3}\frac{a^3-b^3}{1-v^2}$$
$$+ \frac{4(1-v)}{(1-2v)(1+v)}\left[\frac{b}{d}\psi(a,b) - \Psi(a,b) - \frac{\pi}{4}\frac{a^2}{d^2} - \frac{\pi}{16}ln\left(1 - \frac{4a^2}{d^2}\right)\right], \tag{4b}$$

---

[1] Unfortunately, a detailed comparison with the results by Dintwa et al. (2008) is problematic since the principal "calibration curve" (Eq. (8) and Fig. 13 in that paper) describing the deflection between the Hertz model and the Finite Element Analysis (FEA) contains a dimension error. Therefore, we could compare only some particular results, such as values in Fig. 11. For instance, the normal force $N(h)$ at point $h = 0.01d$ calculated via FEA is 6% higher that the Hertz value, while the rod model presents an overestimation of 16%. Comparison for higher deformations can provide FEA values closer to the rod model, if a sudden increase in Fig. 11 is not a numerical artifact. Further, the analysis presented by Jefferson et al. (2002) concerns truncated spheres (consolidated granular material) and thus is suitable for qualitative comparison only. The question of quantitative comparison remains hereby open.
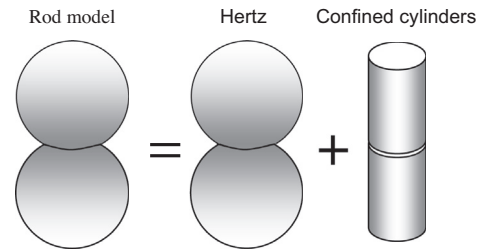
where

$$\psi(a,b) = \sqrt{1 - \frac{4b^2}{d^2}} \, \mathrm{atanh}\left(\sqrt{\frac{4a^2 - 4b^2}{d^2 - 4b^2}} \right) - \frac{2}{d}\sqrt{a^2 - b^2},$$

$$\Psi(a,b) = \frac{1}{d}\int_0^b \psi(a,r)dr.$$

It is of interest to note that the solution of the tangential problem uses the half-space approximation while the normal solution does not. Indeed, stress distribution Eq. (3c) applied to an elastic half-space produces displacement different from Hertzian form Eq. (3b). This disparity can be attributed to the fact that for increasing normal force the normal deformation experiences an unlimited growth that eventually violates the frameworks of the Hertz approximation, while the increase of tangential force and deformation is limited by the total sliding of particles. Therefore, with small but realistic values $\mu \approx 0.1$ particles strongly deformed in the normal direction but relatively weakly deformed in the tangential direction can be observed. This fact provides some grounds for using the half-space approximation for the tangential problem.

The rod model is one of the possible high-strain approximations for normal contact between spheres. The objective of this paper is to develop a method for automatically solving tangential problems in such approximations. It is interesting to note that the analytical technique utilized in the Jäger theorem is perfectly suited here even though theorem itself is not applicable for model/empirical normal stress distributions. In addition, the derivations here are much simpler than those which are needed to obtain Eqs. (4a), (4b) in the framework of Mindlin's methodology.

3. Shift and torsion contact problems

3.1. Tangential shift for a model normal stress distribution

The starting point of the technique (Jäger, 1995) is the solution to the problem of a tangential shift by distance δ_0 of a plat circular punch firmly adhered to an elastic half-space:

$$\tau_0 = \frac{q}{\sqrt{a^2 - \rho^2}}, \quad \delta_0 = \frac{\pi(2-v)(1+v)}{2E}q \tag{5}$$

Then, the solution for a shift of the contact zone at point $\rho < a$ is expressed as a superposition of infinitesimal components Eq. (5) with a weight $q(s)ds$ for a punch of radius s, $b \leqslant s \leqslant a$. The choice of the s-range automatically guarantees that all points within the stick zone $\rho < b$ have equal displacements. So, the integration of Eq. (5) provides the following result for the traction distribution $\tau(\rho)$ and the tangential displacement δ of the stick zone (see Eq. (29) by Jäger, 1995):

$$\tau(\rho) = \begin{cases} \int_\rho^a \frac{q(s)ds}{\sqrt{s^2 - \rho^2}}, & \rho \geqslant b, \\ \int_b^a \frac{q(s)ds}{\sqrt{s^2 - \rho^2}}, & \rho \leqslant b, \end{cases} \tag{6}$$

$$\delta = \frac{\pi(2-v)(1+v)}{2E}\int_b^a q(s)ds, \qquad \rho \leqslant b. \tag{7}$$

The boundary condition in the stick zone $\rho < b$ has already been taken into account. The boundary condition in the slip zone $b \leqslant \rho \leqslant a$ is given by the Coulomb friction law $\tau = \mu\sigma$ that results in the integral equation for the weight function $q(s)$:

$$\mu\sigma(a,\rho) = \int_\rho^a \frac{q(s)ds}{\sqrt{s^2 - \rho^2}}. \tag{8}$$

Further, Jäger (1995) considers the analogous expression for the normal stress $\sigma(a,\rho)$, and, because of the identity of the corresponding integrals derive the result Eq. (2).

In the case of a model stress distribution $\sigma(a,\rho)$ that does not present an exact solution to any normal problem, the relationship Eq. (2) is not applicable. However, Eq. (8) is the integral Abel equation that can be inverted (see, for instance, a handbook by Korn and Korn, 1961) for any model distribution $\sigma(a,\rho)$ (in fact, only the continuous derivability of $\sigma(a,\rho)$ is required):

$$q(s) = -\mu\frac{2}{\pi}\frac{d}{ds}\int_s^a \frac{\rho\sigma(a,\rho)d\rho}{\sqrt{\rho^2 - s^2}}. \tag{9}$$

It is easy to obtain by substituting Eq. (9) into Eq. (7) that

$$\delta = -\mu\frac{(2-v)(1+v)}{E}\int_b^a \frac{\rho\sigma(a,\rho)d\rho}{\sqrt{\rho^2 - b^2}}. \tag{10}$$

The last expression, by inserting the normal stress Eq. (3c) for the rod model, coincides with the result Eq. (4a) obtained with the help of the traditional approach by Mindlin and Cattaneo that requires quite tedious calculations.

For traction in the stick zone $\rho < b$ Eq. (6) and Eq. (9) yield

$$\tau(\rho) = -\frac{2\mu}{\pi}\int_b^a \frac{ds}{\sqrt{s^2 - \rho^2}}\frac{d}{ds}\left(\int_s^a \frac{r\sigma(a,r)}{\sqrt{r^2 - s^2}}dr\right). \tag{11}$$

The tangential force is presented then as a sum of two components,

$$T = T_1 + T_2, \tag{12}$$

$$T_1 = 4\mu\int_0^b \rho d\rho \int_b^a \frac{ds}{\sqrt{s^2 - \rho^2}}\frac{d}{ds}\left(\int_s^a \frac{r\sigma(a,r)}{\sqrt{r^2 - s^2}}dr\right), \tag{13}$$

$$T_2 = -2\pi\mu\int_b^a \sigma(a,\rho)\rho d\rho. \tag{14}$$

By changing the order of integration in Eq. (13) we obtain

$$T_1 = 4\mu\int_b^a ds(s - \sqrt{s^2 - b^2})\frac{d}{ds}\left(\int_s^a \frac{r\sigma(a,r)}{\sqrt{r^2 - s^2}}dr\right), \tag{15}$$

which, by integrating by parts, is transformed to the expression

$$T_1 = -4\mu b\int_b^a \frac{r\sigma(a,r)}{\sqrt{r^2 - b^2}}dr - 4\mu\int_b^a ds\int_s^a \frac{r\sigma(a,r)}{\sqrt{r^2 - s^2}}dr$$
$$+ 4\mu\int_b^a \frac{sds}{\sqrt{s^2 - b^2}}\left(\int_s^a \frac{r\sigma(a,r)}{\sqrt{r^2 - s^2}}dr\right). \tag{16}$$

The first integral here coincide with displacement δ (Eq. (10)). After changing of the order of integration in the last two integrals, Eq. (16) becomes

$$T_1 = \frac{4b\delta E}{(2-v)(1+v)} - 4\mu\int_b^a r\sigma(a,r)\left[\frac{\pi}{2} - \mathrm{asin}\left(\frac{b}{r}\right)\right]dr$$
$$+ 2\pi\mu\int_b^a r\sigma(a,r)dr. \tag{17}$$

Combination of Eq. (14) and Eq. (17) produces the following result for the total tangential force:

$$T = \frac{4Eb}{(2-v)(1+v)}\delta - 4\mu\int_b^a \rho\sigma(a,\rho)\left[\frac{\pi}{2} - \mathrm{asin}\left(\frac{b}{\rho}\right)\right]d\rho. \tag{18}$$

Expressions (10) and (18) link tangential displacement δ and tangential force T in an implicit manner and represent a solution to the tangential contact problem for any model normal stress distribution $\sigma(a,\rho)$.

For a weak tangential action when the slip zone is practically absent ($b \to a$), the solutions Eqs. (10), (18) linearize so that the result does not depend on the normal stress distribution anymore:

$$T = \frac{4Ea}{(2-v)(1+v)}\delta. \tag{19}$$

If, inversely, the slip zone reaches the contact center, the stick zone disappears that results in total sliding with the Coulomb friction law satisfied in the form

$$T = 2\pi\mu \int_0^a \sigma(a,\rho)\rho d\rho \equiv \mu N. \tag{20}$$

In a particular case of the rod model with the normal stress distribution Eq. (3c), the result Eq. (18) produces the expression

$$\frac{T}{\mu Ed^2} = \frac{4(b/d)}{(2-v)(1+v)}\frac{\delta}{\mu d} + \frac{4}{d^2}\int_b^a \left[\frac{\pi}{2} - \mathrm{asin}\left(\frac{b}{\rho}\right)\right]$$
$$\left[\frac{4\sqrt{a^2-\rho^2}}{\pi d(1-v^2)} + \frac{1-v}{(1-2v)(1+v)}ln\left(\frac{d^2-4\rho^2}{d^2-4a^2}\right)\right]\rho d\rho \tag{21}$$

that, as it is possible to see, coincides with Eq. (4b).

3.2. Torsion for model normal stress distributions

The analysis discussed in Section 3.1 has been suggested and implemented by Jäger (1995) for rotational action. For particles compressed by a normal force N creating the normal stress distribution $\sigma(a,\rho)$, the rotation angle θ and the moment of force (torque) M relative to the axis connecting the particles centers are linked with the following relationships:

$$\theta = -\mu\frac{1+v}{E}\int_b^a \frac{\sigma(a,\rho)}{\sqrt{\rho^2-b^2}}d\rho, \tag{22}$$

$$M = \frac{8}{3}\mu \int_b^a ds \int_s^a d\rho \frac{s^2\rho}{\sqrt{\rho^2-s^2}}\frac{\partial\sigma(a,\rho)}{\partial\rho}, \tag{23}$$

where b is, as previously, the radius of boundary between the stick and slip zones. The integration in Eq. (23) can be performed analytically that, after a series of transformations, results in a simpler form

$$M = \frac{8Eb^3}{3(1+v)}\theta$$
$$- 4\mu \int_b^a \sigma(a,\rho)\left[\rho^2\left(\frac{\pi}{2} - \mathrm{asin}\left(\frac{b}{\rho}\right)\right) + b\sqrt{\rho^2-b^2}\right]d\rho. \tag{24}$$

The above expressions (22) and (24) in the limit of small θ produces the linear relation between M and θ

$$M = \frac{8Ea^3}{3(1+v)}\theta \tag{25}$$

that correspond to result by Reissner and Sagoci (see Mindlin, 1949). The upper limit for the torque ($b \to 0$) is given by the Coulomb friction law

$$M_{max} = 2\pi\mu \int_0^a \sigma(a,\rho)\rho^2 d\rho. \tag{26}$$

However, whereas in the tangential shift problem the limiting force $T_{max} = \mu N$ (Eq. (20)) is achieved with a finite value of δ, in the torsion problem M_{max} corresponds to the rotation angle $\theta \to \infty$. This fact is determined by a singular character of the dependency $\theta(b)$ in Eq. (22) at $b \to 0$. The analysis of Eq. (22) in that limit provides the following result:

$$\frac{\theta}{\mu} = c_1 ln\left(\frac{b}{d}\right) + c_2 + o(1),$$

with

$$c_1 = \frac{1-v}{1-2v}ln\left(1 - \frac{4a^2}{d^2}\right) - \frac{4(a/d)}{\pi(1-v)},$$

$$c_2 = \frac{4(a/d)}{\pi(1-v)}\left[\ln\left(\frac{4a}{d}\right) - 1\right]$$
$$- \frac{1-v}{1-2v}\left[\frac{1}{2}\mathrm{dilog}\left(1 - \frac{4a^2}{d^2}\right) + \ln\left(\frac{2a}{d}\right)\ln\left(1 - \frac{4a^2}{d^2}\right)\right].$$

Thus, total sliding ($b = 0$) is unachievable by pivoting; even for very high θ there is always a tiny stick area $0 < \rho < b$. This feature is not surprising since the central points $\rho = 0$ of the particles are always at rest and can never rotate by definition.

3.3. Numerical examples and discussion

The general solutions to shift (Eqs. (10), (18)) and torsion (Eqs. (22), (24)) problems are applicable for any normal stress distributions $\sigma(a,\rho)$ including those that do not represent any exact solution to the normal problem but are obtained from physical considerations. An example of the rod model is illustrated in Fig. 2. Since the rod model includes a virtual presence of strained cylinders in additions to Hertzian spheres, the load–displacement curve is generally stiffer that in the Hertz case. In particular, in the shift problem, total sliding occurs at higher values of the tangential displacement and force (Fig. 2a), similarly to saturation of the dependency $M(\theta)$ for the torsion problem (Fig. 2b).
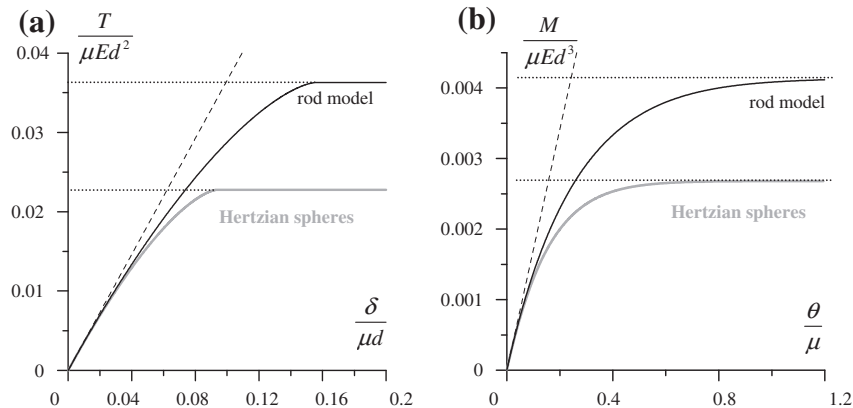

Fig. 2. (a) Dependency of tangential force T on tangential displacement δ obtained for the rod model with the help of Eqs. (4a), (4b); (b) torque M as a function of rotation angle θ in accordance to Eqs. (22), (24). In both figures: dashed lines correspond to asymptotes for $\delta \ll$ (or $\theta \ll 1$), dotted lines denote maximum force and torque achieved at full sliding. Here $a = 0.2d$ and $v = 0.25$.

An interesting feature can be found in the very structure of the general solutions obtained. The tangential or rotational properties of the system depend only on the part of the normal stress distribution located in the slip zone. In other words, the integration in Eqs. (10), (18), (22), (24) is performed over section $[b, a]$ only. This is an expected result since the absence of slip is equivalent to the presence of intact material in the zone $[0, b]$. In this sense, the system of two spheres behaves as a single particle consisting of two fused spheres, with the only difference that the fusion zone actually evolves depending on the applied tangential (rotational) action.

4. Varying tangential/rotational and constant normal actions

4.1. Memory diagrams

Here we call "action" both force and displacement in the shift problem, and both torque and rotation angle, in the torsion problem. The resulting expressions Eqs. (10), (18) and Eqs. (22), (24) connect actions with the stick–slip boundary b that actually represents an argument in the solution. For definiteness, we shall speak of the displacement-driven tangential shift problem i.e. a situation when displacement δ is given and force T is unknown. It is essential that the results obtained in Section 3 applicable only for constant normal and tangential actions. Below we shall consider a situation when the normal compression is fixed and tangential displacement δ varies in an arbitrary way. First al all, for increasing δ the Coulomb friction law in the slip zone has to be fulfilled in the form $\tau(\rho) = \mu|\sigma(a, \rho)|$, while for decreasing δ it should read $\tau(\rho) = -\mu|\sigma(a, \rho)|$. Thus, the initial loading and subsequent reloadings lead to different situations: in the former case the contact zone was initially free of traction, whilst in the latter one it already supported some nonzero traction that should be compensated for prior to any further application of traction. This feature was considered in full detail by Aleshin and Van Den Abeele (2012); an automatic compensation for the residual traction is provided by the method of memory diagrams that enables us to take into account arbitrary changes in δ in a universal way. A short summary of the method of memory diagrams is given by the same authors (Aleshin and Van Den Abeele, 2013). In the present case, the consideration is much simpler since normal action is not a function of the tangential one but assumed constant.

The method uses a kind of a general scheme of memory organization in the contact system (memory diagram) that replaces in the analysis the actual traction distribution. After passing a number of extrema in the δ-protocol, the traction distribution becomes a piecewise-smooth function whose nodes correspond to some previous stick–slip boundaries b. These values called here memory points are "memorized" at the moments when an extremum is passed i.e. when the time derivative $d\delta/dt$ changes sign $I = \mathrm{sgn}(d\delta/dt)$. Fig. 2 illustrates a typical traction distribution $\tau(\rho)$ after passing a sequence of extrema; the corresponding memory diagram is also plotted. Constant compression prohibits the appearance of overloading (Aleshin and Van Den Abeele, 2012) i.e. a situation when the rate of the contact radius a increase is larger than the rate of slip inward propagation, so that slip does not develop at all. Thus, in our case, the solution always remains hysteretic since slip is always present in the outer annulus $b < \rho < a$. A chain b_m ($m = 1..M$) of previous stick–slip boundaries determines the memory effects in the system. The memory diagram in that case is defined as a sequence of points b_m and the point b, supplemented by alternating signs I_m ($I_m = -I_{m-1}$) and the current sign I (see Fig. 3).
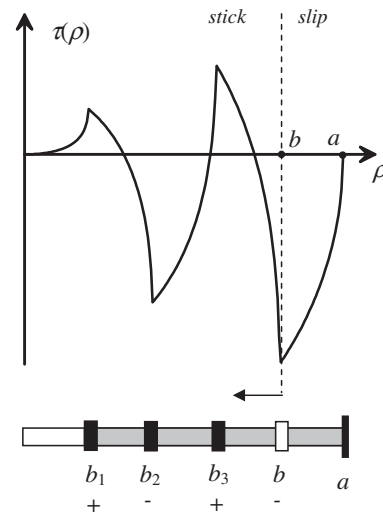

Fig. 3. Typical traction distribution $\tau(\rho)$ obtained after a series of slip reversals and correspondent memory diagram. Points b_1–b_3 do not move, point b shifts to the left as slip propagates towards the center.

4.2. Initial hysteresis curve

The solution to the problem depends on whether some memory points are present in the diagram ($M > 0$) or not ($M = 0$). In the latter case corresponding to the initial hysteresis curve, the result has already been obtained in Section 3; here we rewrite it as

$$\begin{cases} \delta = \bar{\delta}(b) \iff b = \bar{\delta}^{-1}(\delta) \\ T = \bar{T}(b) \end{cases}, \tag{27}$$

where $\bar{\delta}(b)$ and $\bar{T}(b)$ are given by Eqs. (10), (18):

$$\bar{\delta}(b) = -\mu \frac{(2-v)(1+v)}{E} \int_b^a \frac{\rho\sigma(a, \rho)d\rho}{\sqrt{\rho^2 - b^2}}, \tag{28}$$

$$\bar{T}(b) = \frac{4Eb}{(2-v)(1+v)} \bar{\delta}(b) - 4\mu \int_b^a \rho\sigma(a, \rho)\left[\frac{\pi}{2} - \mathrm{asin}\left(\frac{b}{\rho}\right)\right] d\rho. \tag{29}$$

The inverse function $\bar{\delta}^{-1}(\delta)$ in Eq. (27) can be calculated analytically for some known distributions of the normal stress $\sigma(a, \rho)$, such as the Hertz case, or numerically for any model $\sigma(a, \rho)$. It is always possible as the direct function $\bar{\delta}(b)$ is monotonous (for an increasing displacement slip propagates towards the center).

Solution (27) is written for increasing and positive δ and can be easily modified to include decreasing and negative δ as well,

$$\begin{cases} b = \bar{\delta}^{-1}(|\delta|) \equiv \bar{\delta}^{-1}(I\delta) \\ T = I\bar{T}(|b|) \equiv I\bar{T}(Ib) \end{cases}. \tag{30}$$

Note that for the initial hysteresis curve increasing argument means positive, and decreasing argument means negative.

4.3. Other hysteresis curves

Leaving the initial hysteresis curve leaves also some residual traction in the contact zone. It can be taken into account by adding a factor of two into the solution,

$$\begin{cases} \delta = \delta_M + 2I\bar{\delta}(Ib) \iff b = \bar{\delta}^{-1}(\frac{1}{2}I(\delta - \delta_M)) \\ T = T_M + 2I\bar{T}(Ib) \end{cases}, \tag{31}$$

where the extremum point (δ_M, T_M) is known. The fact that slip inward propagation not only "writes" the traction $\tau(\rho) = \mu|\sigma(a,\rho)|$ but erases the residual stress is reflected in the memory diagram (Fig. 3) as grey filling. In a more general case then overloading is possible, one has to introduce more filling styles in order to reproduce various regimes of the system's evolution.

4.4. Evolution of memory diagrams

Thus we have found the solutions corresponding to a given memory diagram. These expressions Eqs. (30), (31) have to be supplemented by an algorithm controlling the evolution of memory diagrams. During the evolution two events may happen: (i) passing an extremum results in the creation of a new memory point, and (ii) slip inward propagation i.e. decreasing b can erase some of existing memory points.

In the latter case, again, two situations are possible. If b reaches b_M with $M = 1$ (the only memory point in the diagram), this point b_1 is deleted and the solution follows the initial hysteresis curve (Eq. (30)). But if b reaches b_M with $M > 1$, not one but two memory points should be deleted. Indeed, consider the solution for the traction

$$\tau(\rho) = \tau_{M-2}(\rho) + 2\bar{\tau}(b_{M-1}, \rho) - 2\bar{\tau}(b_M, \rho) + 2\bar{\tau}(b, \rho) \quad (32)$$

obtained analogously to Eq. (31) with

$$\bar{\tau}(b,\rho) = -\frac{2\mu}{\pi} \int_b^a \frac{ds}{\sqrt{s^2-\rho^2}} \frac{d}{ds}\left(\int_s^a \frac{r\sigma(a,r)}{\sqrt{r^2-s^2}}dr\right) \quad (33)$$

according to Eq. (11). Here $I = 1$ for definiteness. Then, assuming $b = b_M$ cancels two last terms in Eq. (30). The remaining expression

$$\tau(\rho) = \tau_{M-2}(\rho) + 2\bar{\tau}(b_{M-1}, \rho)$$

satisfies the Coulomb friction law in the zone $b_{M-1} < \rho < a$. Consequently, this zone is the actual slip annulus and the actual stick–slip boundary b equals b_{M-1}. For further increase in δ, slip will continue expanding downwards starting from b_{M-1}. This actually means that b_{M-1} is erased, too. The described property is called the s-jump rule by Aleshin and Van den Abeele, 2012, or b-jump rule from the point of notations used here.

In Fig. 4 we illustrate the algorithm governing the evolution of memory diagrams in a particular case of constant compression. For numerical implementation, some discretization of δ-protocol has to be used. The procedure enables us to make subsequent time steps and redefines variables δ, b, and T at each step. The discretization step should be small enough in order to locate precisely the positions of extrema and the moments of time when the previously memorized extrema are erased. Anyway, the step is δ-protocol should be less than the distance between any memory points b_{m-1} and b_m, otherwise algorithm in Fig. 4 cannot guarantee the fulfillment of the conditions $b_1 < ... < b_m < ... < b_M$.

A numerical example for the rod model is given in Fig. 5. Each of two curves (one for the rod model and one for Hertzian spheres) has an internal loop. Such structure results from a protocol in which an initial curve is followed by a cycle that consists in loading, partial unloading and then reloading, in terms of displacement δ or force T. As previously (Fig. 2) the dependency $T(\delta)$ generally has stiffer behavior for the rod model, since it contains a virtual deformable cylinder in addition to Hertzian spheres. In fact the δ-range in Fig. 5 is selected such that the Hertz system almost reaches the total sliding threshold, whereas this threshold for the rod model is 67% higher (with the parameter values $a = 0.2d$ and $v = 0.25$).
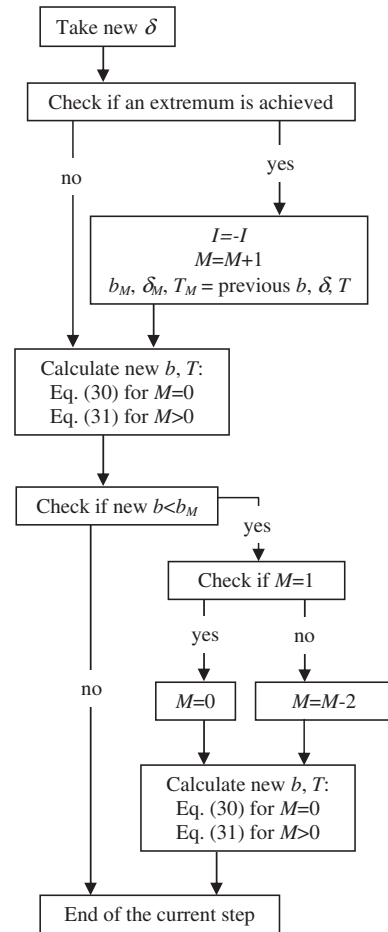

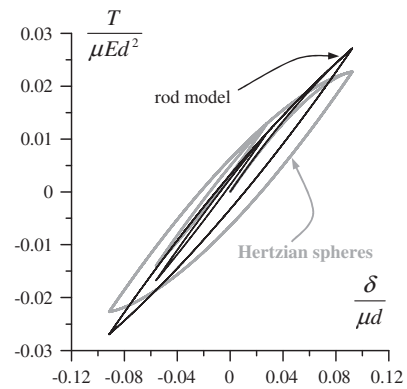Fig. 4. Algorithm of the method of memory diagrams in a particular case of constant normal compression.

Fig. 5. Hysteresis curves $T(\delta)$ for exemplar δ-protocol with one internal loop. Here $a = 0.2d$ and $v = 0.25$.

5. Conclusions

In this paper, we have extended the formalism initially proposed by Jäger (1995) for solving contact shift and torsion problems to the case of an arbitrary normal stress distribution. An important feature of the method is its applicability to model normal stresses which do not satisfy exactly the equations of contact mechanics but result from physical considerations. The tangential displacement and force are expressed via integral representations containing the normal stress distribution. These expressions

provide an explicit link between force and displacement through a changing lower limit of integration (boundary between stick and slip zones). The torsion problem is solved in an analogous way.

Another essential aspect of the solution is in the possibility to use the method of memory diagrams that accepts an arbitrary protocol of a drive parameter instead of particular evolution cases, such as loading–unloading, etc., usually considered in contact mechanics. On the other hand, the result discussed here is only applicable at constant normal compression.

Acknowledgements

References

Aleshin, V., Van Den Abeele, K., 2012. Hertz–Mindlin problem for arbitrary oblique 2D loading: general solution by memory diagrams. J. Mech. Phys. Solids 60 (1), 14–36.

Aleshin, V., Van Den Abeele, K., 2013. General solution to the Hertz–Mindlin problem via Preisach formalism. Int. J. Non-Linear Mech. 49, 15–30.

Barber, J.R., Davies, M., Hills, D.A., 2011. Frictional elastic contact with periodic loading. Int. J. Solids Struct. 48, 2041–2047.

Boltachev, G.Sh., Volkov, N.B., 2012. Compaction and elastic unloading of nanopowders under the granular dynamic method. Powder Metallurgy and Metal Ceramics 51, 260–266.

Boltachev, G.Sh., Volkov, N.B., Kaygorodov, A.S., Loznukho, V.P., 2011. The Peculiarities of Uniaxial Quasistatic Compaction of Oxide Nanopowders. Nanotechnologies in Russia 6, 639–646.

Boltachev, G.Sh., Volkov, N.B., Zubarev, N.M., 2012. Tangential interaction of elastic spherical particles in contact. Int. J. Solids Struct. 49, 2107–2114.

Capriz, G., Giovine, P., Mariano, P.M., 2008. Mathematical Models of Granular Matter. Springer, Berlin.

Cattaneo, C., 1938. Sul contatto di due corpi elastici: distribuzione locale degli sforzi. Accad. Lincei Rend. 27 (6), 342–348.

Dintwa, E., Tijskens, E., Ramon, H., 2008. On the accuracy of the Hertz model to describe the normal contact of soft elastic spheres. Granular Matter 10, 209–221.

Duran, J., 1999. Sands, Powders, and Grains: An Introduction to the Physics of Granular Materials. Springer, New York.

Hertz, H., 1881. Über die Berührung fester elastischer Korper. J. Reine Angew. Math. 92, 156–171.

Jäger, J., 1995. Axisymmetric bodies of equal material in contact under torsion or shift. Arch. Appl. Mech. 65, 478–487.

Jäger, J., 2002. New analytical and numerical results for two-dimensional contact profiles. Int. J. Solids Struct. 39, 959–972.

Jefferson, G., Haritos, G.K., McMeeking, R.M., 2002. The elastic response of a cohesive aggregate – a discrete element model with coupled particle interaction. J. Mech. Phys. Solids 50, 2539–2575.

Korn, G., Korn, T., 1961. Mathematical Handbook for Scientists and Engineers. McGraw-Hill, New York.

Mavko, G., Mukerji, T., Dvorkin, J., 1998. The Rock Physics Handbook. Cambridge University Press, Cambridge.

Mindlin, R.D., 1949. Compliance of elastic bodies in contact. J. Appl. Mech. 16, 259–268.